Chapter 4
Quantification of Spike-LFP Synchronization

Zhaohui Li and Xiaoli Li

4.1 Introduction

The advent of multielectrode arrays makes it possible to simultaneously record the spiking activity of multiple neurons and neural ensembles, which offers an important avenue to investigate fundamental issues about the neural coding (Galashan et al. 2011; Stafford et al. 2009). The resulting voltage signals are generally separated into two types: one is the spikes or action potentials, which are fired by neurons and identified by high-pass filtering, detecting, and sorting, and another is the local field potentials (LFPs), which are the total synaptic current in the neuronal circuit and obtained by low-pass filtering the original wideband signal (Mizuseki et al. 2009; Perelman and Ginosar 2007). The interaction between the spikes of single neurons, i.e., spike trains, and the ongoing LFP oscillations is becoming a hot topic in neuroscience, because it allows us to study how the activities of individual neurons are related to those of the larger-scale networks in which they are embedded. Its significance has been shown to be associated with high-level brain functions, such as attention (Chalk et al. 2010; Fries et al. 2001), memory (Harris et al. 2002; Le Van Quyen et al. 2008; Lee et al. 2005), motor task (Courtemanche et al. 2002; Hagan et al. 2012; van Wingerden et al. 2010), and sensory processing (Eggermont and Smith 1995; Fries et al. 1997; Pienkowski and Eggermont 2011 Xu et al. 2012).

Z. Li
School of Information Science and Engineering, Yanshan University, Qinhuangdao 066004, China
e-mail: lizhaohui@ysu.edu.cn

X. Li (✉)
State Key Laboratory of Cognitive Neuroscience and Learning & IDG/McGovern Institute for Brain Research, Beijing Normal University, Beijing 100875, China

Center for Collaboration and Innovation in Brain and Learning Sciences, Beijing Normal University, Beijing 100875, China
e-mail: xiaoli@bnu.edu.cn

X. Li (ed.), *Signal Processing in Neuroscience*, DOI 10.1007/978-981-10-1822-0_4

4.2 Spike Field Coherence

4.2.1 Spike-Triggered Average and Spike Field Coherence

A typical method for studying spike-LFP interaction is the spike field coherence (SFC), which measures synchronization between spike trains and LFPs as a function of frequency and takes values between 0 % (complete lack of synchronization) and 100 % (complete synchronization) (Fries et al. 2001; Fries et al. 1997). The SFC can be used to describe the strength of synchronization between spike times and a particular phase of the LFP oscillation at a certain frequency. It has been employed to investigate the memory formation in humans (Rutishauser et al. 2010), the neural mechanism of visual attention in macaque monkeys (Chalk et al. 2010; Fries et al. 2001), the stimulus-specific synchronization in primary visual cortex of awake-behaving cats (Siegel and Konig 2003), and other brain functions (Fries et al. 2002; Issa and Wang 2011; Lewandowski and Schmidt 2011; Tiesinga et al. 2004; Wang et al. 2011). An important advantage of the SFC is that it is independent on the LFP power and spike rate (Fries et al. 2001).

The SFC is a function of frequency and obtained by computing the ratio of power spectrum of the spike-triggered average (STA) over the average of power spectrum of the LFP fractions (Fries et al. 1997). Thus, the SFC is independent on the LFP power and spike rate (Fries et al. 2001). Suppose that the spike train of a neuron is denoted as $S = [s_1, s_2, \ldots s_m]$, where m is the spike number. $V = [v_1, v_2, \ldots v_m]$ is the set of LFP segments, where v_i is the samples of the LFP signal in the window $[s_i - T/2,\ \ s_i + T/2]$. Here, T is the duration of the window. The STA is constructed by averaging the LFP fractions within windows that centered on the spikes. Then, the power spectrum of STA (PSTA) is defined as

$$\mathrm{PSTA} = \Psi\left(\frac{1}{m}\sum_{i=1}^{m} v_i\right), \tag{4.1}$$

where Ψ denotes the operation for calculating the power spectrum. Next, to describe the power of every frequency component in the LFP segments that used to construct the STA, i.e., v_i with $i = 1, 2, \ldots, m$, the average power spectrum of v_i (spike-triggered power spectrum or STP) is (Fries et al. 1997; Rutishauser et al. 2010)

$$\mathrm{STP} = \frac{1}{m}\sum_{i=1}^{m} [\Psi\,(v_i)]. \tag{4.2}$$

Then, the SFC is defined as [17]

$$\mathrm{SFC} = \frac{\mathrm{PSTA}}{\mathrm{STP}} \times 100\%. \tag{4.3}$$

The STP and PSTA can be computed with many methods. For instance, multitaper analysis is a powerful and robust method to estimate single-trial spectrum (Jarvis

and Mitra 2001), which can be performed by using the Chronux toolbox (Bokil et al. 2010). The multitaper method is employed in this chapter for spectrum analysis of the simulated and experimentally recorded LFP signals.

4.2.2 Bursty Spike Trains and Weighted Spike Field Coherence

The SFC reflects the synchronization between spike trains and LFPs at different frequencies. However, it does not work well for bursty spike trains and LFPs at high frequency band, which will be shown in the following section. A burst can be defined as a temporary increase in the firing rate of spikes from the background activity (Cocatre-Zilgien and Delcomyn 1992; Palm 1981; Robin et al. 2009). As the mechanism for generating bursts is mentioned, it is commonly accepted that small depolarization keeps the cell silent, moderate depolarization makes the cell fire single spikes, and large depolarization causes the cell to discharge in burst mode. Thus, bursts code the same neural information as single spikes but with higher reliability (Harris et al. 2001; Lisman 1997). With this understanding, the first spike in each burst is selected and used to represent the burst as event (Kepecs and Lisman 2003; Swadlow and Gusev 2001).

When all spikes in the bursts are used to calculate the coherence, this operation will decrease the SFC values even if there is strong phase-locked synchronization between bursty spike trains and LFPs at high frequency band. To overcome this drawback, an improvement for the algorithm of SFC is introduced in this chapter. That is, multiple copies of the first spike in each burst are used to compute the SFC. The number of the copies is determined by the number of spikes per burst. Since this is analogous to the process of weight, the modified approach is referred to as weighted spike field coherence (WSFC). To evaluate the performance of this method, it is applied to both simulation data and real neurobiological signals recorded in the hippocampus of rats.

The WSFC method allows only the first spike in every burst enter into the computation of PSTA and STP. To emphasize the difference between single spikes and bursts, multiple copies of the first spikes in bursts are used. In this way, the first spike timing represents the occurrence of the burst, and the weighting procedure (multiple copies of the first spike) reflects the properties of the burst. Then, the WSFC is defined as

$$\mathrm{WSFC} = \frac{\mathrm{PWSTA}}{\mathrm{WSTP}} \times 100\,\%, \tag{4.4}$$

where the PWSTA is the power spectrum of weighted STA and the WSTP denotes the weighted spike-triggered power spectrum of LFP. The "weighted" means that the LFP segments around the first spikes in bursts are reused in the calculation of STA and STP, and the "weight" is related to the spike number per burst. The main difference between the two methods is that WSFC uses the first spike in burst

multiple times rather than all the spikes used by SFC. An important advantage of this operation is that it can remove the influence of the second and later spikes in bursts on the computation of SFC. In other words, the WSFC method is immune to the effect of burst.

Similar to the SFC, the WSFC is a population method and cannot be calculated for single spikes. It suffers from the effect of spike count used in the computation as well. Thus, it is necessary to minimize or avoid the bias raised by the amount of spikes. Two measures may be adopted. One is to use enough spikes (>50 generally) to calculate the WSFC. Another is to ensure that the spike counts in different conditions are equal. In addition, two parameters should be identified before calculating the SFC and WSFC. First, the traces of LFP to construct the STA are set to be 960 ms in the simulations, with the aim of examining low frequencies. For the real data in this study, a relatively short window of 480 ms is used focusing on the gamma band frequencies. To summarize, the window length is selected depending on the following principle: long enough to make reliable estimate for the power spectrum and relatively short to represent the dynamics of LFP signal in the desired band. Next, in the simulations, the spectrum is estimated by using multitaper method with a time-bandwidth product of four and seven tapers, resulting in a spectral resolution (half bandwidth) of 4.2 Hz. In the analysis of real data, due to the short window of 480 ms, we use a time-bandwidth product of three and five tapers in order to get a relatively smaller spectral resolution of 6.25 Hz. It means that we should choose an appropriate time-bandwidth product and taper count to make a good compromise between the spectral resolution and the benefit of the spectral estimate.

4.2.3 Simulation and Application

4.2.3.1 Simulation Results

To simulate the real extracellular recoding, the LFP signal is generated by summing multiple sine waves with different frequencies, amplitudes, and phases (Rutishauser et al. 2010). The frequencies range from 1 Hz to 100 Hz with a step of 1 Hz, focusing on the LFP in gamma band and below. The amplitudes of the components are inversely proportional to their frequencies. The phases are randomly selected from $[0\ \ 2\pi]$. In addition, a white Gaussian noise with the signal-to-noise ratio of 3 dB is added to the composite oscillation. Thus, the generated artificial LFP signal follows the 1/f power distribution. The phase-locked spikes that fired by simulated individual neurons locate at a certain phase of the underlying oscillation and skip cycles at random, while the non-phase-locked spikes occur randomly. The simulated bursts consist of two to six spikes. The interspike intervals (ISIs) in the bursts range from 3 to 10 ms. The amount of the burst is quantified by burst index, which is defined as the ratio of spikes in bursts to all spikes (Mizuseki et al. 2011, 2012). To avoid the bias caused by the number of spikes (Fell et al. 2001; Grasse and Moxon 2010), 200 spikes are generated for each realization.

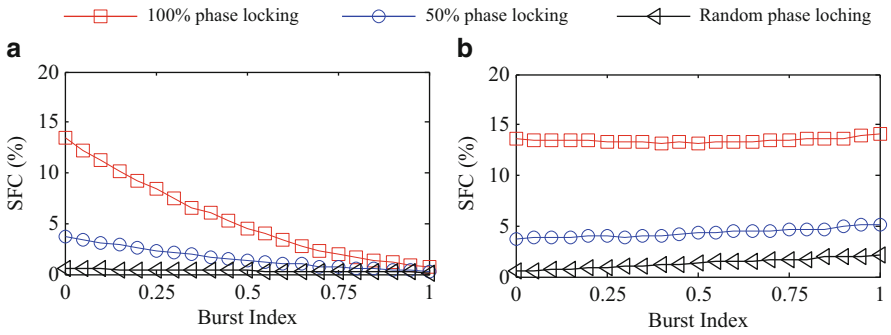

Fig. 4.1 The SFC between bursty spike train and LFP for different phase-locked cases. (**a**) Spikes or bursts are phased locked to 50-Hz component. (**b**) Spikes or bursts are phased locked to 5-Hz component

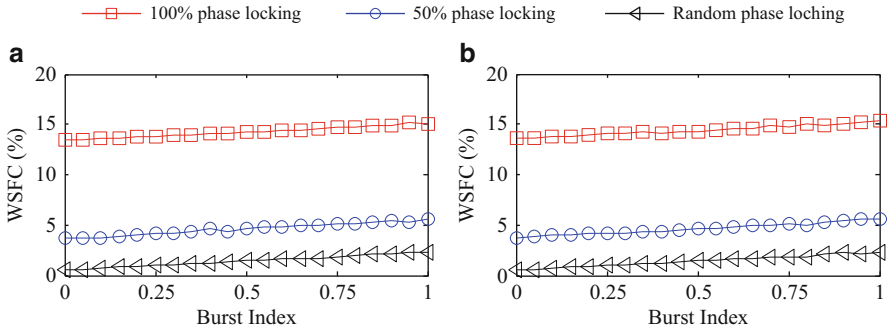

Fig. 4.2 The WSFC between bursty spike train and LFP for different phase-locked cases. (**a**) The phase locking is represented between spikes or bursts and 50-Hz component. (**b**) The phase locking is represented between spikes or bursts and 5-Hz component

By using the simulated LFP signal, the effect of bursts in spike trains on the calculation of SFC and WSFC is investigated, and the advantage of WSFC for estimating the coherence between bursty spike trains and LFPs is demonstrated. The SFC and WSFC are calculated in three cases: 100 % spikes are locked to a certain phase of specified components (e.g., 50 Hz and 5 Hz) in the simulated LFP signal (100 % phase locked), 50 % spikes are phased locked (50 % phase locked), and spikes are fired randomly (non-phase locked), where the spikes include single spikes and first spikes in bursts. The mean values of SFC and WSFC at the two frequencies versus the burst indexes are plotted in Figs. 4.1 and 4.2. For the 50-Hz component, the SFC is strongly reduced by the bursts that occurred in spike trains for both 100 % and 50 % phase-locked cases, while it keeps at the chance level for the random phase locking, as shown in Fig. 4.1a. It means that the bursts do not lead to spurious increase of the SFC for random spikes, but can severely reduce the SFC values for spikes phase locked to high-frequency components. For

the 5-Hz component, the decrease of the SFC also presents in the 100 % and 50 % phase-locked cases, but with smaller amplitude. However, the SFC increases a little for the random phase locking, as illustrated in Fig. 4.1b. It implies that the bursts exert relatively small effect on the SFC estimate for spikes phase locked to low-frequency components. All simulations are implemented by using 200 spikes, which means that the decrease of the SFC is indeed caused by the location rather than the amount of spikes.

On the other hand, the WSFC method using the first spikes effectively eliminates this influence caused by bursts for both low and high frequencies. Due to the reuse of first spikes in bursts, the amplitude of the STA gets larger as a function of the number of bursts involved. Consequently, the WSFC presents a slight increase with the increasing of bursts in spike trains, as shown in Fig. 4.2a, b. However, the relative difference in WSFC between conditions almost remains the same, which is meaningful for the comparison between different phase-locked cases.

Furthermore, the influence of the bursts at different frequencies is examined. The given nine frequencies are as follows: 5 Hz in theta band, 10 Hz in alpha band, 20 Hz in beta band, and 30 Hz, 40 Hz, 50 Hz, 60 Hz, 70 Hz, and 80 Hz in gamma band. The single spikes and first spikes in bursts are presumed to fire exactly at a certain phase of these component oscillations. The influence is quantified by the coefficient of variation (CV) of the SFC or WSFC magnitudes for different burst indexes. As shown in Fig. 4.3a, b, the SFC between spike trains and LFPs in gamma frequency band is prone to be affected by the bursts for 100 % and 50 % phase-locked cases. Whereas for the low frequencies, e.g., 5 Hz and 10 Hz, the bursts in spike trains exert very little effect on the computation of SFC, on the other hand, the WSFC has a relatively more robust performance for both high and low frequencies. The effect of bursts under the random phase locking is illustrated in Fig. 4.3c. The SFC and WSFC measure performs similarly to each other. Although the variation of WSFC is relatively large, it does not imply a reduction of the WSFC performance. As explained before, these variations are represented in different locked conditions with similar increasing tendencies, providing a reliable comparison of the coherence between different conditions. This is also demonstrated by the values of CV in different phase-locked cases. The lower degree of the phase locking, the smaller mean of the WSFC at different burst indexes and the larger CVs for frequencies take

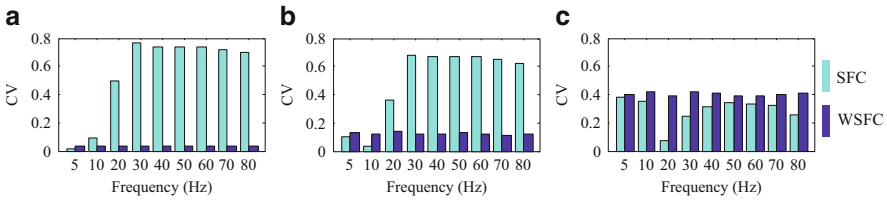

Fig. 4.3 Effect of burst on the SFC and the WSFC when spikes or bursts phase locked to different frequency components. (**a**) 100 % phase locking. (**b**) 50 % phase locking. (**c**) Random phase locking

on. To summarize, the WSFC is an efficient tool to reveal the coherence between spike trains and LFPs, particularly in high frequency band.

4.2.3.2 Application to Real Data

The data set consists of simultaneous recordings of cells in layer CA1 of the right dorsal hippocampus of three Long-Evans rats, which were implanted with a 4-shank or 8-shank silicon probe. After recovery from surgery (about 1 week) and training (at least 3 days), the physiological signals were recorded during the open field tasks in which the rats chased randomly dispersed drops of water or pieces of Froot Loops on an elevated square platform. The signals were amplified (1000x), band-pass filtered (1 Hz–5 kHz), and sampled continuously at 20 kHz. Then, the LFPs were down-sampled to 1250 Hz. The offline spike sorting was performed automatically. The details about the behavioral experiment and data collection can be found in (Mizuseki et al. 2009). A subset of the data set is analyzed in this study (in particular, ec013.527 at http://crcns.org/data-sets/hc/hc-2).

In hippocampus, gamma frequency oscillations (30–80 Hz) have been suggested to underlie various cognitive functions, such as attention selection (Bauer et al. 2006; Fries et al. 2001), memory (Fell et al. 2001; Howard et al. 2003; van Vugt et al. 2010), and sensory perception (Colgin et al. 2009; Muzzio et al. 2009). Moreover, it has been reported that the firing patterns of pyramidal cells in hippocampus are significantly phase locked to gamma oscillations in behaving rats (Colgin et al. 2009; Csicsvari et al. 2003; Senior et al. 2008). Here, we examine that whether this phase locking can be characterized by the WSFC and SFC methods. In the recordings of the data set used in this study, the pyramidal cells exhibit firing patterns of single spikes and complex spike bursts. A segment ($150 \sim 400$ s) of the recordings used for the analysis of coherence is shown in Fig. 4.4a, b, containing the gamma band LFP signal and the neuronal activity (neuron 37 in the selected data set).

In order to preserve the timing relationship between spikes and LFP, the gamma band-pass filtering is performed digitally with zero-phase shift using the EEGLAB toolbox (Delorme and Makeig 2004). Then, we estimate the WSFC and SFC as a function of time (sliding window of 10s advanced in steps of 5 s), respectively. A series of two or more consecutive spikes with <10-ms ISIs is considered as a burst in this study (Mizuseki et al. 2011; Senior et al. 2008). Figure 4.4c shows the burst index in every window. To guarantee sufficient statistical power, we select the windows containing at least 50 single spikes and bursts for the calculation of coherence (Rutishauser et al. 2010). For statistical purposes, the results are converted to z-scores. The surrogate spike trains are created by perturbing every spike with a random time in a window of 30 ms around the original spikes. The statistical significance is set conservatively at $z > 1.96$ for the level $p < 0.05$. In Fig. 4.4d, e, the z-transformed WSFC and SFC are plotted versus time, respectively, and the horizontal line indicates the significant level. Obviously, the traditional method, i.e., SFC which uses all spikes in bursts, fails to descript the phase locking

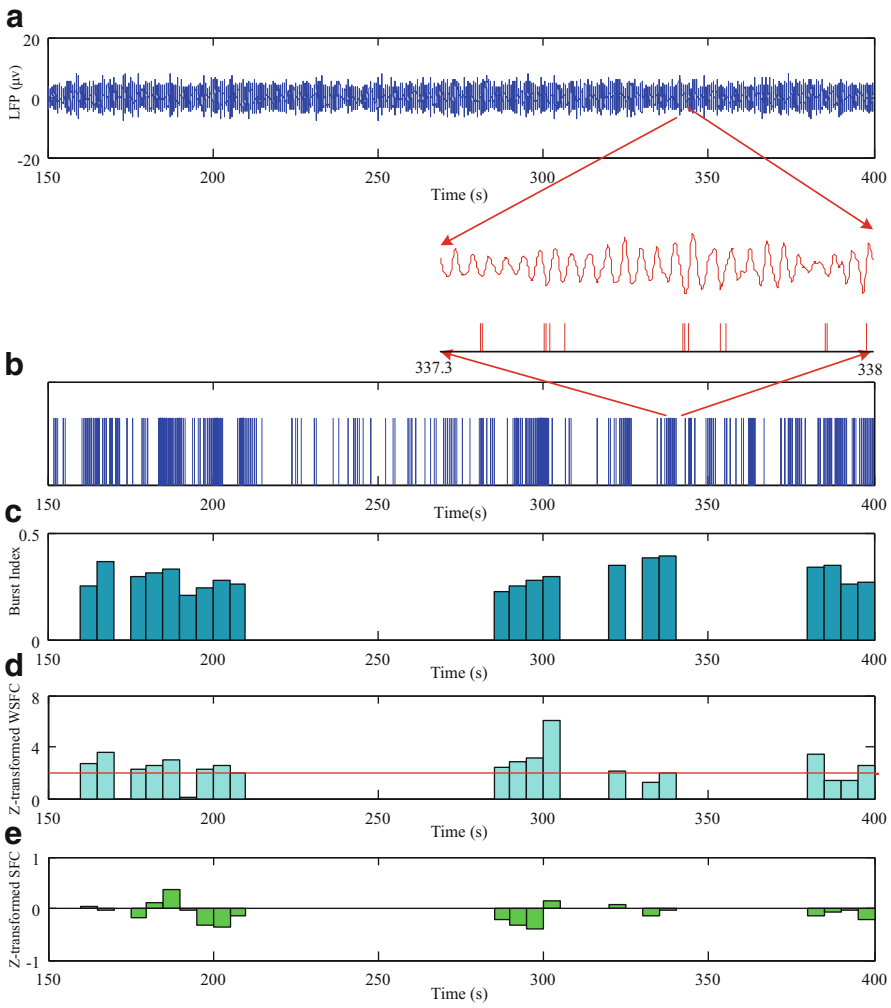

Fig. 4.4 The WSFC and SFC applied to real data. (**a**) A segment of the recorded LFP signal. (**b**) Spiking activities of neuron 37 in the segment. *Vertical lines* indicate the occurrence of spikes fired by the neuron. (**c**) Burst index for windows with >50 spikes. (**d**) Z-transformed WSFC for each selected window. The *red horizontal line* indicates the significant level of $p < 0.05$. (**e**) Z-transformed SFC for each selected window. The coherence in the two plots (*d*) and (*e*) is obtained by using the average of the WSFC and SFC within gamma band, respectively

between the spike train and LFP in gamma band, while the modified method, i.e., WSFC which utilizes the copies of first spikes in bursts, characterizes this relationship effectively. We also found similar results for other data sets, which further demonstrate the performance of WSFC to uncover the relationship between activities of pyramidal cells in hippocampus and LFP in gamma band; the results for other data sets are shown in the supporting document.

4.3 Spike-Triggered Correlation Matrix Synchronization

Spikes and LFP are acquired from the signal recorded by a microelectrode. The former are fired by neurons and identified by high-pass filtering, detection, and sorting. The latter reflects the total effects of the synaptic currents in the neuronal circuit and is obtained by low-pass filtering the original wideband signal. Several rhythms of LFP are generated through inhibitory networks that produce periodic fluctuations in the intracellular potential of the target postsynaptic neurons such that the excitability of these neurons varies within one period of the rhythm, which can be used to synchronize the spiking of neurons (Buzsaki and Wang 2012; Ray 2014). Also, it is reported that spikes can be inferred from LFP in the primary visual cortex of monkeys (Rasch et al. 2008). Furthermore, LFP is thought to mainly reflect the summed transmembrane currents flowing through the neurons within a local region around the microelectrode tip (Buzsaki et al. 2012; Reimann et al. 2013), and its phase is widely adopted to characterize the spike-LFP synchronization (Colgin et al. 2009; Csicsvari et al. 2003; Fries et al. 2001). In view of the above considerations, we suggest that a specific variation of LFP phase causes an individual neuron to fire spikes and consequently generate the spike-LFP synchronization.

4.3.1 Correlation Matrix and Spike-LFP Synchronization

Several spike-LFP synchronization measures have been introduced in the past few years, e.g., the phase histogram (Csicsvari et al. 2003), phase locking (Colgin et al. 2009), spike field coherence (Fries et al. 2001), and coherency (Pesaran et al. 2002). However, these measures are dependent upon the total number of spikes, which renders comparison of spike-LFP synchronization across experimental contexts difficult. Often, different experimental conditions yield substantially different numbers of spikes. Thus, it is necessary and urgent to develop an unbiased measure for characterizing the synchronization between spikes and LFP. In 2010, a circular statistics, pairwise phase consistency (PPC), has been proposed. It is a bias-free and consistent estimator of spike-LFP synchronization (Vinck et al. 2010). Unfortunately, as shown below, the performance of PPC severely deteriorates in the presence of spike noise. In this chapter, we present a new measure for estimating spike-LFP synchronization, which is independent of the total number of spikes and robust against spike noise. The main idea of the method is to take LFP segments centered on each spike (spike-triggered LFPs) as multichannel signals and calculate the index of spike-LFP synchronization by constructing a correlation matrix. Thus, this method is referred to as spike-triggered correlation matrix synchronization (SCMS).

Suppose that the spike train (i.e., a series of spikes) fired by a neuron is denoted as $S = [s_1, s_2, \ldots s_n]$, where s_i $(i = 1, 2, \ldots, n)$ is the spiking time and n is the number of spikes. $V = [v_1, v_2, \ldots v_n]$ is the set of LFP segments, where v_i $(i = 1, 2, \ldots, n)$ denotes the samples of the LFP signal in the time window $[s_i - T/2,\ \ s_i + T/2]$

and T is the duration of the LFP segments. First, extract the instantaneous phase of every LFP segment by Hilbert transform. For a signal $v(t)$, the analytic signal $\zeta(t)$ is a complex function of time, and it is defined as

$$\zeta(t) = v(t) + j\tilde{v}(t) = A(t)e^{j\phi(t)}, \tag{4.5}$$

where the function $\tilde{v}(t)$ is the Hilbert transform of $v(t)$:

$$v(t) = \frac{1}{\pi}\text{P.V.} \cdot \int_{-\infty}^{+\infty} \frac{v(t)}{t-\tau}\, d\tau. \tag{4.6}$$

P.V. indicates that the integral is taken in the sense of Cauchy principal value (Rosenblum et al. 1996). Thus, the instantaneous phase $\phi_i(t)$ of LFP segment $v_i(t)$ is obtained. Second, construct the correlation matrix $\mathbf{C}$ by calculating the phase-locking value (PLV) between pairs of LFP segments, i.e.,

$$c_{ij} = \left| \frac{1}{N} \sum_{k=1}^{N} e^{j\left(\phi_i(t_k) - \phi_j(t_k)\right)} \right|, \tag{4.7}$$

where N denotes the number of samples in the time window and $\mathbf{C}$ is a real symmetric matrix. Then, the eigenvalue decomposition of $\mathbf{C}$ is given by

$$C\, u_i = \lambda_i\, u_i, \tag{4.8}$$

where λ_i are the eigenvalues, with $\lambda_1 \geq \lambda_2 \geq \cdots \geq \lambda_n$, and u_i are the eigenvectors corresponding to λ_i. Finally, in order to obtain a normalized value of spike-LFP synchronization which is independent of the number of spikes, we randomize all spike-triggered LFP segments to compute a surrogate correlation matrix $\mathbf{R}$ (Li et al. 2007). The surrogate data is generated by randomly shuffling the order of the original signals (Theiler et al. 1992). Similarly, we can obtain the ordered eigenvalues of matrix $\mathbf{R}$. Repeating this randomization and computation M times (we select $M = 100$ in this work), the mean and standard deviation (SD) of the maximum eigenvalues are denoted as $\overline{\lambda}_1'$ and s_1, respectively. Then, the normalized spike-LFP synchronization can be computed by the following equation:

$$\eta = \begin{cases} \left(\lambda_1 - \overline{\lambda}_1'\right) / \left(n - \overline{\lambda}_1'\right) & \text{if } \lambda_1 > \left(\overline{\lambda}_1' + K \times s_1\right) \\ 0 & \text{otherwise} \end{cases}, \tag{4.9}$$

where K is a constant that determines the threshold and $K = 3$ is selected for 99 % confidence intervals (Li et al. 2007).

The reason for the choice of the maximum eigenvalue (λ_1 and $\overline{\lambda}_1'$) is in the following. Li et al. noted that when multichannel signals are acquired from a local region, the first synchronization index, which corresponds to the maximum eigenvalue, is appropriate for indicating the global synchronization (Li et al. 2007). Moreover, as spikes and LFP are recorded by the same microelectrode, the spike-

triggered LFPs can be considered as signals from one region of synchronization. Thus, it is justifiable to use the first synchronization index to characterize the spike-LFP synchronization.

In the SCMS algorithm, a parameter (i.e., the window length of the LFP segments) should be determined before its application. It is possible that there are other spikes immediately before or after a specific spike. These spikes may alter the frequency and phase of the LFP (Zanos et al. 2011). This supports the selection of a short window. However, the algorithm uses the similarity of the variation in LFP phase as the mechanism for the calculation of spike-LFP synchronization. Consequently, a longer window improves the accuracy of the similarity calculation. Considering this trade-off, we used a window of 20 ms in the analysis of simulated and real data.

4.3.2 Simulation and Application

4.3.2.1 Simulation Results

To test the properties of the algorithm, simulated LFP was generated by summing multiple sine waves with different frequencies, amplitudes, and phases (Rutishauser et al. 2010). The frequencies ranged from 1 to 100 Hz with a step of 1 Hz, thereby focusing on the LFP in the gamma band and below. The amplitudes of the components were inversely proportional to their frequencies. The phases were randomly selected from $[0\ 2\pi]$. Synchronized spikes fired by simulated individual neurons were located at a certain phase of the summed LFP waveform. These simulated neurons skipped cycles at random. The total number of synchronized spikes was denoted by ϑ_p. Additionally, non-synchronized spikes occurred randomly, and their amount was denoted by ϑ_n. The strength of spike-LFP synchronization was determined by the ratio $R = \vartheta_p / \left(\vartheta_p + \vartheta_n\right)$, e.g., $R = 1$ implies perfect synchronization and $R = 0$ indicates complete non-synchronization.

First, the effect of the total number of spikes on the algorithm's output was investigated. The number of spikes ranged from 10 to 100 with a step of 5. The strength of simulated spike-LFP synchronization was set to 0.25, 0.5, or 0.75. Figure 4.5 shows the mean value of the SCMS output for different numbers of spikes, with 100 realizations for each number. As can be seen, the SCMS output almost does not change with the sample size. This property is of crucial importance when making comparisons between different experimental conditions.

Second, the robustness of the SCMS method against noise in the spike trains was studied. Three types of noise were considered: jitter noise (a shift of spiking time), missing spikes (false negatives), and extra spikes (false positives). Jitter noise may appear in stochastic biological processes, such as synaptic transmission and spike propagation in a neural network. The noise due to missing and extra spikes is primarily caused by external processes such as the firing of other neurons, errors in the spike sorting procedure, and electrical artifacts (Asai and Villa 2008). We compare the SCMS method with the pairwise phase consistency (PPC) method.

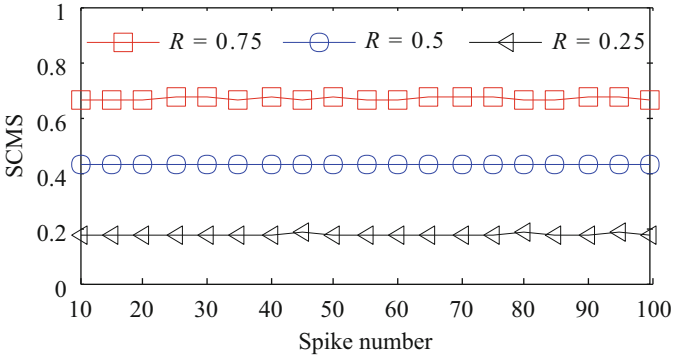

Fig. 4.5 Effect of the total number of spikes on the output of the SCMS method

Jitter noise was added to the spike trains via shifting every spike by a time normally distributed in an interval. The strength of jitter noise was quantified by the interval length. The number of spikes in the simulation was set to 50. As shown in Fig. 4.6a, b, both the SCMS and the PPC are affected by jitter noise, and their output values decrease as the interval of jitter increases. However, the output of SCMS decreases more slowly compared to that of PPC. Moreover, we are still able to visually distinguish between the different levels of spike-LFP synchronization in the SCMS output even as the jitter interval grows to 20 ms. In contrast, it becomes difficult to observe a clear distinction between different levels of synchronization by looking at the PPC output when the interval is larger than 5 ms. Once the data acquisition procedures, recording system, and the spike detection method have been determined, the jitter noise of different neurons is about the same in scale. Thus, when comparing the spike-LFP synchronization between different experimental conditions or between different pairs of neurons and LFP signals, the SCMS measure is able to provide more significant results.

Noise due to extra spikes was quantified by the number of independent spikes randomly inserted into spike trains. In the simulation, the original number of spikes was 20, and the number of extra spikes ranged from 2 to 30 with a step of 2. As shown in Fig. 4.6c, d, the SCMS and PPC outputs decrease with the number of extra spikes. Due to the random insertion of independent spikes, the strength of the simulated spike-LFP synchronization reduces, and consequently the two outputs decrease. It is difficult to distinguish between different synchronization strengths by looking at the output of the PPC method when a large amount of extra spikes is present. In comparison, the output of the SCMS method indicates differences between the synchronization levels for even the largest amount of extra spikes.

The noise due to missed spikes was quantified by the number of randomly deleted spikes. In the simulation, the original number of spikes was 50, and the number of missed spikes ranged from 2 to 30, with a step of 2. Figure 4.6e, f show that the two methods are basically unaffected by the number of missed spikes. That is to say, they are robust against the noise due to missed spikes. The underlying reason is that the

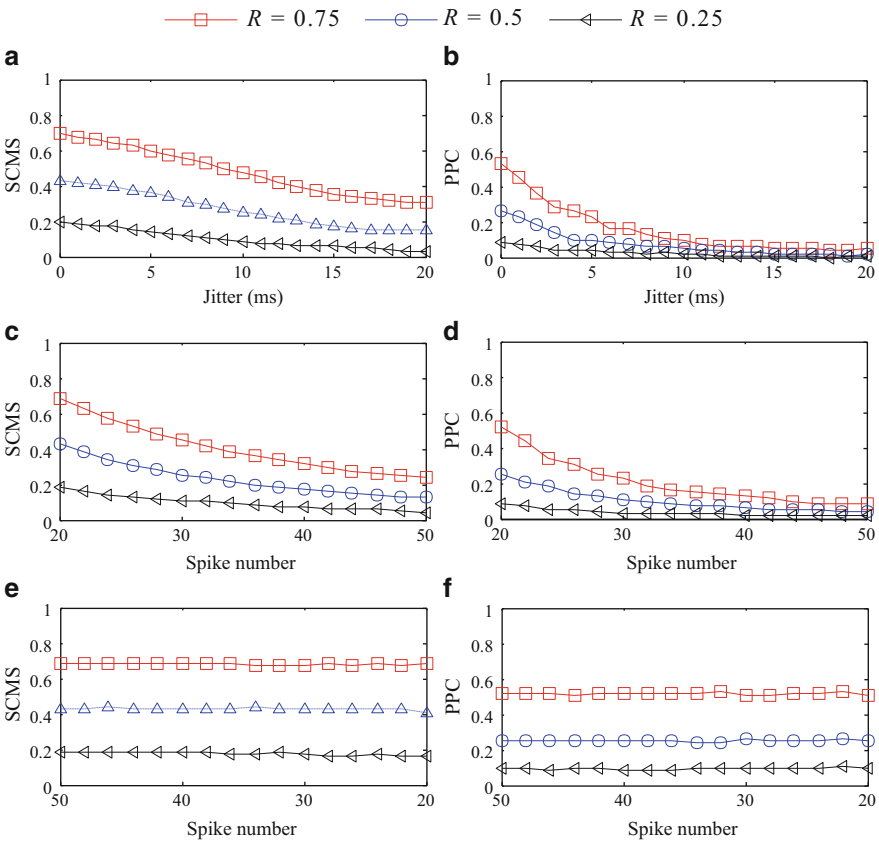

Fig. 4.6 Effect of noise in the spike trains on SCMS and PPC. The simulated spike-LFP synchronization strength was 0.25, 0.5, or 0.75. There were 100 realizations for each strength. (**a**) Mean SCMS output and (**b**) mean PPC output as a function of jitter noise. (**c**) Mean SCMS output and (**d**) mean PPC output versus the number of extra spikes. (**e**) Mean SCMS output and (**f**) mean PPC output versus the number of missed spikes

random deletion of spikes does not alter the strength of spike-LFP synchronization, but just reduce the total number of spikes. Since the two methods are not biased by the total number of spikes, they are both resistant to noise arising from missed spikes.

4.3.2.2 Application to Real Data

In this section, the SCMS method was applied to data recorded from rhesus monkey. All procedures were conducted in compliance with the National Institutes of Health Guide for the Care and Use of Laboratory Animals and were approved by the

Institutional Animal Care and Use Committee of Beijing Normal University. Data was recorded from a male adult monkey (*Macaca mulatta*). After the animal had been trained in a simple fixation task, a 6×8 multielectrode array (with electrode length of 0.5–0.6 mm, interelectrode spacing of 0.4 mm, and typical electrode impedances of a few hundred kiloohms at 1 kHz; Blackrock Microsystems) was implanted into V1 corresponding to eccentricities between 2.0° and 5.0° in the lower visual field. LFP and spike data were recorded at 30 kHz using a 128-channel acquisition system (Cerebus; Blackrock Microsystems). Visual stimuli were generated by a stimulus generator (ViSaGe; Cambridge Research Systems) on a 22-in. CRT monitor (Iiyama Vision Master Pro 514) at a viewing distance of 100 cm. Drifting sinusoidal gratings (99 % contrast; spatial frequency, 2 cycle/deg; temporal frequency, 4 Hz) were displayed within a circular patch of 4° visual angle in diameter, covering the visual field locations of all recording sites. The gratings drifted in different directions between 0 and 360°, in 22.5° steps in a pseudorandom order. The stimulus was presented for 2 s and repeated eight times.

To identify spikes fired by neurons, the recorded signals were filtered with a band-pass filter of 300–3000 Hz. Then, spikes were detected using a threshold method (Quiroga et al. 2004). We did not use spike sorting in this work. Due to the robustness of the method against noise in spike trains, it was not necessary to implement spike sorting in the data preprocessing. For LFPs, the recorded signals were filtered with a band-pass filter of 30–80 Hz, because our concentration was on the synchronization between spikes and LFPs in the gamma band. To preserve the phase relationship between spikes and LFP, gamma band-pass filtering was performed digitally with a zero-phase shift using the EEGLAB toolbox (Delorme and Makeig 2004).

Orientation selectivity is an emergent property of neurons in the primary visual cortex (V1) (Hubel and Wiesel 1962, 1968). Most studies focused on the response of individual neurons to investigate the mechanisms of this selectivity (Priebe and Ferster 2012; Ringach et al. 1997; Shapley et al. 2003). Neuronal oscillations in the gamma band (30–80 Hz) have been suggested to play a central role in feature binding or establishing channels for neural communication (Ray and Maunsell 2010). With increasing interest in and popularity of LFP analysis, oscillations in LFP gamma band have been used to study orientation selectivity (Berens et al. 2008; Xing et al. 2012). In this chapter, we examined whether the spike-LFP synchronization exhibits orientation selectivity in macaque V1 by using the SCMS method. Orientation selectivity based on spike-LFP synchronization is quantified by circular variance (CV), which is a global measure of the shape of the orientation tuning curve and defined as (Batschelet 1981)

$$\Gamma = 1 - \frac{\left|\sum_k r_k \exp\left(i2\theta_k\right)\right|}{\sum_k r_k}, \tag{4.10}$$

where r_k denotes the mean spike-LFP synchronization in response to a drifting grating with angle θ_k. The angles θ_k spanned the range from 0 to 360 ° with

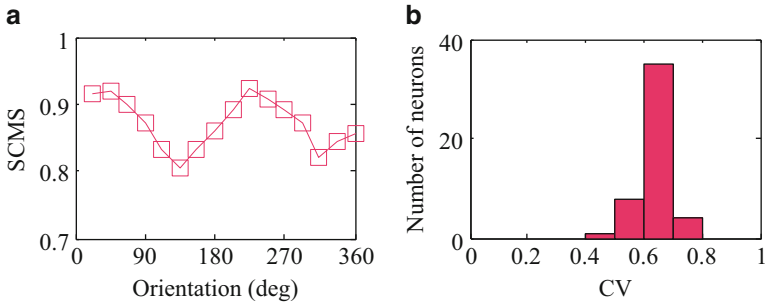

Fig. 4.7 Application of SCMS to data recorded from the visual cortex of a rhesus monkey. (**a**) The orientation tuning curve, calculated using spike-LFP synchronization as a substitute for firing rate, of a neuron (electrode #17) in V1. (**b**) The histogram of circular variance (CV) values, quantifying significance of orientation selectivity, of the 48 recorded neurons from V1

equally spaced intervals (22.5 ° in this work). According to circular statistics, $\Gamma < 0.9$ means that the orientation selectivity of a neuron to the drifting grating is significant. Figure 4.7a shows the tuning curve based on spike-LFP synchronization of a neuron in V1. Clearly, two troughs can be observed and the tuning curve shows a regular pattern as a function of the orientation. This means that the spike-LFP synchronization of this neuron is sensitive to the orientations of the drifting gratings. As shown in Fig. 4.7b, the CV of all 48 recorded neurons in V1 is less than 0.8, and the great majority (75 %) is located in the range from 0.6 to 0.7. This implies that the recorded neurons' spike-LFP synchronization exhibits significant orientation selectivity.

4.4 Conclusion

In this chapter, we introduced two methods to estimate the synchronization between the spiking activity of individual neurons and the LFP of neural ensembles. The WSFC is a correcting measure of a widely used SFC method which underestimates the coherence between bursty spike trains and LFPs, especially in high frequency band. The WSFC method allows only the first spike in every burst to enter into the calculating procedure, aiming to eliminate the influence of the other spikes. Moreover, it utilizes multiple copies of the first spike to highlight the difference between single spike and burst. This "weighting" operation preserves the inherent characteristic of burst, i.e., series of spikes raised by a large depolarization. Both simulation and experimental results show that the WSFC method performs better than SFC for investigating the relationship between bursty spike trains and high frequency band LFPs. Also, it can be used to analyze any spike trains and LFPs. Furthermore, a potential application of the WSFC is to study whether bursts enhance

the coherence between spike trains and LFPs. Briefly, the WSFC is a promising method to uncover details of the neural coding.

Moreover, we introduced a new method, spike-triggered correlation matrix synchronization (SCMS), for characterizing the synchronization between spike trains and rhythms present in LFP. We demonstrated that the SCMS is not sensitive to the total number of spikes in the calculation. In addition, it is superior to another unbiased measure (PPC) in resisting spike noise arising from jitter and extra spikes. Thus, the SCMS is a promising measure for estimating spike-LFP synchronization. By applying the SCMS method to neuronal data recorded from macaque primary visual cortex, we demonstrate that spike-LFP synchronization can be used to explore the mechanism of orientation selectivity.

References

Asai Y, Villa AE. Reconstruction of underlying nonlinear deterministic dynamics embedded in noisy spike trains. J Biol Phys. 2008;34:325–40.

Batschelet E. Circular statistics in biology. London: Academic; 1981.

Bauer M, Oostenveld R, Peeters M, Fries P. Tactile spatial attention enhances gamma-band activity in somatosensory cortex and reduces low-frequency activity in parieto-occipital areas. J Neurosci. 2006;26:490–501.

Berens P, Keliris GA, Ecker AS, Logothetis NK, Tolias AS. Comparing the feature selectivity of the gamma-band of the local field potential and the underlying spiking activity in primate visual cortex. Front Syst Neurosci. 2008;2:2.

Bokil H, Andrews P, Kulkarni JE, Mehta S, Mitra PP. Chronux: a platform for analyzing neural signals. J Neurosci Methods. 2010;192:146–51.

Buzsaki G, Wang XJ. Mechanisms of gamma oscillations. Annu Rev Neurosci. 2012;35:203–25.

Buzsaki G, Anastassiou CA, Koch C. The origin of extracellular fields and currents – EEG, ECoG, LFP and spikes. Nat Rev Neurosci. 2012;13:407–20.

Chalk M, Herrero JL, Gieselmann MA, Delicato LS, Gotthardt S, Thiele A. Attention reduces stimulus-driven gamma frequency oscillations and spike field coherence in V1. Neuron. 2010;66:114–25.

Cocatre-Zilgien JH, Delcomyn F. Identification of bursts in spike trains. J Neurosci Methods. 1992;41:19–30.

Colgin LL, Denninger T, Fyhn M, Hafting T, Bonnevie T, Jensen O, Moser MB, Moser EI. Frequency of gamma oscillations routes flow of information in the hippocampus. Nature. 2009;462:353–7.

Courtemanche R, Pellerin JP, Lamarre Y. Local field potential oscillations in primate cerebellar cortex: modulation during active and passive expectancy. J Neurophysiol. 2002;88:771–82.

Csicsvari J, Jamieson B, Wise KD, Buzsaki G. Mechanisms of gamma oscillations in the hippocampus of the behaving rat. Neuron. 2003;37:311–22.

Delorme A, Makeig S. EEGLAB: an open source toolbox for analysis of single-trial EEG dynamics including independent component analysis. J Neurosci Methods. 2004;134:9–21.

Eggermont JJ, Smith GM. Synchrony between single-unit activity and local field potentials in relation to periodicity coding in primary auditory cortex. J Neurophysiol. 1995;73:227–45.

Fell J, Klaver P, Lehnertz K, Grunwald T, Schaller C, Elger CE, Fernandez G. Human memory formation is accompanied by rhinal-hippocampal coupling and decoupling. Nat Neurosci. 2001;4:1259–64.

Fries P, Roelfsema PR, Engel AK, Konig P, Singer W. Synchronization of oscillatory responses in visual cortex correlates with perception in interocular rivalry. Proc Natl Acad Sci U S A. 1997;94:12699–704.
Fries P, Reynolds JH, Rorie AE, Desimone R. Modulation of oscillatory neuronal synchronization by selective visual attention. Science. 2001;291:1560–3.
Fries P, Schroder JH, Roelfsema PR, Singer W, Engel AK. Oscillatory neuronal synchronization in primary visual cortex as a correlate of stimulus selection. J Neurosci. 2002;22:3739–54.
Galashan FO, Rempel HC, Meyer A, Gruber-Dujardin E, Kreiter AK, Wegener D. A new type of recording chamber with an easy-to-exchange microdrive array for chronic recordings in macaque monkeys. J Neurophysiol. 2011;105:3092–105.
Grasse DW, Moxon KA. Correcting the bias of spike field coherence estimators due to a finite number of spikes. J Neurophysiol. 2010;104:548–58.
Hagan MA, Dean HL, Pesaran B. Spike-field activity in parietal area LIP during coordinated reach and saccade movements. J Neurophysiol. 2012;107:1275–90.
Harris KD, Hirase H, Leinekugel X, Henze DA, Buzsáki G. Temporal interaction between single spikes and complex spike bursts in hippocampal pyramidal cells. Neuron. 2001;32:141–9.
Harris KD, Henze DA, Hirase H, Leinekugel X, Dragoi G, Czurko A, Buzsaki G. Spike train dynamics predicts theta-related phase precession in hippocampal pyramidal cells. Nature. 2002;417:738–41.
Howard MW, Rizzuto DS, Caplan JB, Madsen JR, Lisman J, Aschenbrenner-Scheibe R, Schulze-Bonhage A, Kahana MJ. Gamma oscillations correlate with working memory load in humans. Cereb Cortex. 2003;13:1369–74.
Hubel DH, Wiesel TN. Receptive fields, binocular interaction and functional architecture in the cat's visual cortex. J Physiol. 1962;160:106–54.
Hubel DH, Wiesel TN. Receptive fields and functional architecture of monkey striate cortex. J Physiol. 1968;195:215–43.
Issa EB, Wang X. Altered neural responses to sounds in primate primary auditory cortex during slow-wave sleep. J Neurosci. 2011;31:2965–73.
Jarvis MR, Mitra PP. Sampling properties of the spectrum and coherency of sequences of action potentials. Neural Comput. 2001;13:717–49.
Kepecs A, Lisman J. Information encoding and computation with spikes and bursts. Network. 2003;14:103–18.
Le Van Quyen M, Bragin A, Staba R, Crepon B, Wilson CL, Engel Jr J. Cell type-specific firing during ripple oscillations in the hippocampal formation of humans. J Neurosci. 2008;28:6104–10.
Lee H, Simpson GV, Logothetis NK, Rainer G. Phase locking of single neuron activity to theta oscillations during working memory in monkey extrastriate visual cortex. Neuron. 2005;45:147–56.
Lewandowski BC, Schmidt M. Short bouts of vocalization induce long-lasting fast gamma oscillations in a sensorimotor nucleus. J Neurosci. 2011;31:13936–48.
Li X, Cui D, Jiruska P, Fox JE, Yao X, Jefferys JG. Synchronization measurement of multiple neuronal populations. J Neurophysiol. 2007;98:3341–8.
Lisman JE. Bursts as a unit of neural information: making unreliable synapses reliable. Trends Neurosci. 1997;20:38–43.
Mizuseki K, Sirota A, Pastalkova E, Buzsaki G. Theta oscillations provide temporal windows for local circuit computation in the entorhinal-hippocampal loop. Neuron. 2009;64:267–80.
Mizuseki K, Diba K, Pastalkova E, Buzsaki G. Hippocampal CA1 pyramidal cells form functionally distinct sublayers. Nat Neurosci. 2011;14:1174–81.
Mizuseki K, Royer S, Diba K, Buzsaki G. Activity dynamics and behavioral correlates of CA3 and CA1 hippocampal pyramidal neurons. Hippocampus. 2012;22:1659–80.
Muzzio IA, Levita L, Kulkarni J, Monaco J, Kentros C, Stead M, Abbott LF, Kandel ER. Attention enhances the retrieval and stability of visuospatial and olfactory representations in the dorsal hippocampus. PLoS Biol. 2009;7:e1000140.
Palm G. Evidence, information, and surprise. Biol Cybern. 1981;42:57–68.

Perelman Y, Ginosar R. An integrated system for multichannel neuronal recording with spike/LFP separation, integrated A/D conversion and threshold detection. IEEE Trans Biomed Eng. 2007;54:130–7.
Pesaran B, Pezaris J, Sahani M, Mitra P, Andersen R. Temporal structure in neuronal activity during working memory in macaque parietal cortex. Nat Neurosci. 2002;5:805–11.
Pienkowski M, Eggermont JJ. Sound frequency representation in primary auditory cortex is level tolerant for moderately loud, complex sounds. J Neurophysiol. 2011;106:1016–27.
Priebe NJ, Ferster D. Mechanisms of neuronal computation in mammalian visual cortex. Neuron. 2012;75:194–208.
Quiroga RQ, Nadasdy Z, Ben-Shaul Y. Unsupervised spike detection and sorting with wavelets and superparamagnetic clustering. Neural Comput. 2004;16:1661–87.
Rasch MJ, Gretton A, Murayama Y, Maass W, Logothetis NK. Inferring spike trains from local field potentials. J Neurophysiol. 2008;99:1461–76.
Ray S. Challenges in the quantification and interpretation of spike-LFP relationships. Curr Opin Neurobiol. 2014;31C:111–18.
Ray S, Maunsell JH. Differences in gamma frequencies across visual cortex restrict their possible use in computation. Neuron. 2010;67:885–96.
Reimann MW, Anastassiou CA, Perin R, Hill SL, Markram H, Koch C. A biophysically detailed model of neocortical local field potentials predicts the critical role of active membrane currents. Neuron. 2013;79:375–90.
Ringach DL, Hawken MJ, Shapley R. Dynamics of orientation tuning in macaque primary visual cortex. Nature. 1997;387:281–4.
Robin K, Maurice N, Degos B, Deniau JM, Martinerie J, Pezard L. Assessment of bursting activity and interspike intervals variability: a case study for methodological comparison. J Neurosci Methods. 2009;179:142–9.
Rosenblum MG, Pikovsky AS, Kurths J. Phase synchronization of chaotic oscillators. Phys Rev Lett. 1996;76:1804–7.
Rutishauser U, Ross IB, Mamelak AN, Schuman EM. Human memory strength is predicted by theta-frequency phase-locking of single neurons. Nature. 2010;464:903–7.
Schwartz AB. Cortical neural prosthetics. Annu Rev Neurosci. 2004;27:487–507.
Senior TJ, Huxter JR, Allen K, O'Neill J, Csicsvari J. Gamma oscillatory firing reveals distinct populations of pyramidal cells in the CA1 region of the hippocampus. J Neurosci. 2008;28:2274–86.
Shapley R, Hawken M, Ringach DL. Dynamics of orientation selectivity in the primary visual cortex and the importance of cortical inhibition. Neuron. 2003;38:689–99.
Siegel M, Konig P. A functional gamma-band defined by stimulus-dependent synchronization in area 18 of awake behaving cats. J Neurosci. 2003;23:4251–60.
Stafford BK, Sher A, Litke AM, Feldheim DA. Spatial-temporal patterns of retinal waves underlying activity-dependent refinement of retinofugal projections. Neuron. 2009;64:200–12.
Swadlow HA, Gusev AG. The impact of 'bursting' thalamic impulses at a neocortical synapse. Nat Neurosci. 2001;4:402–8.
Theiler J, Eubank S, Longtin A, Galdrikian B, Doyne Farmer J. Testing for nonlinearity in time series: the method of surrogate data. Physica D Nonlinear Phenomena. 1992;58:77–94.
Tiesinga PH, Fellous JM, Salinas E, Jose JV, Sejnowski TJ. Inhibitory synchrony as a mechanism for attentional gain modulation. J Physiol Paris. 2004;98:296–314.
van Vugt MK, Schulze-Bonhage A, Litt B, Brandt A, Kahana MJ. Hippocampal gamma oscillations increase with memory load. J Neurosci. 2010;30:2694–9.
van Wingerden M, Vinck M, Lankelma JV, Pennartz CM. Learning-associated gamma-band phase-locking of action-outcome selective neurons in orbitofrontal cortex. J Neurosci. 2010;30:10025–38.
Vinck M, van Wingerden M, Womelsdorf T, Fries P, Pennartz CM. The pairwise phase consistency: a bias-free measure of rhythmic neuronal synchronization. Neuroimage. 2010;51:112–22.
Wang Y, Iliescu BF, Ma J, Josic K, Dragoi V. Adaptive changes in neuronal synchronization in macaque V4. J Neurosci. 2011;31:13204–13.

Xing D, Shen Y, Burns S, Yeh CI, Shapley R, Li W. Stochastic generation of gamma-band activity in primary visual cortex of awake and anesthetized monkeys. J Neurosci. 2012;32:13873–80a.

Xu S, Jiang W, Poo MM, Dan Y. Activity recall in a visual cortical ensemble. Nat Neurosci. 2012;15:449–55.

Zanos TP, Mineault PJ, Pack CC. Removal of spurious correlations between spikes and local field potentials. J Neurophysiol. 2011;105:474–86.